SUPPLEMENTAL FIGURES

Figure S1-Related to Figure 1

A Conditional allele of *Pten*

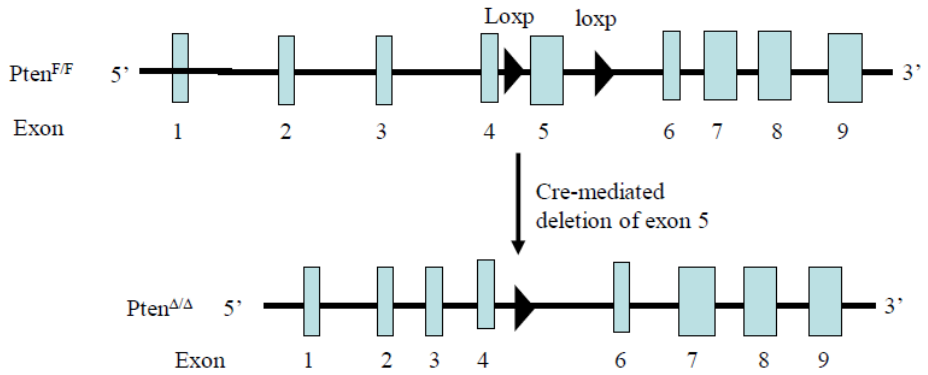

B Conditional allele of *Trp53*

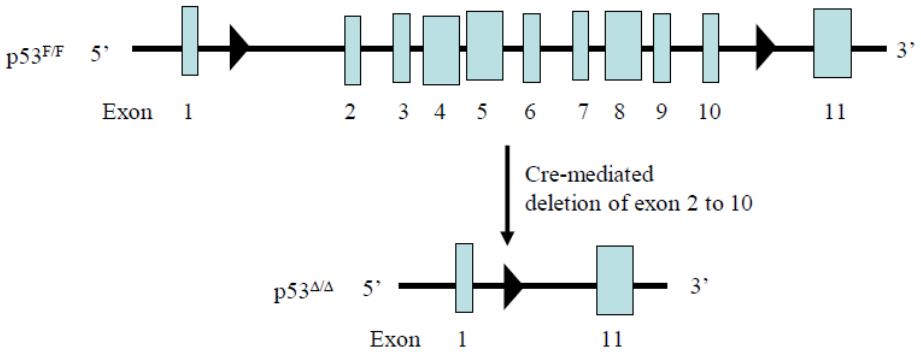

C

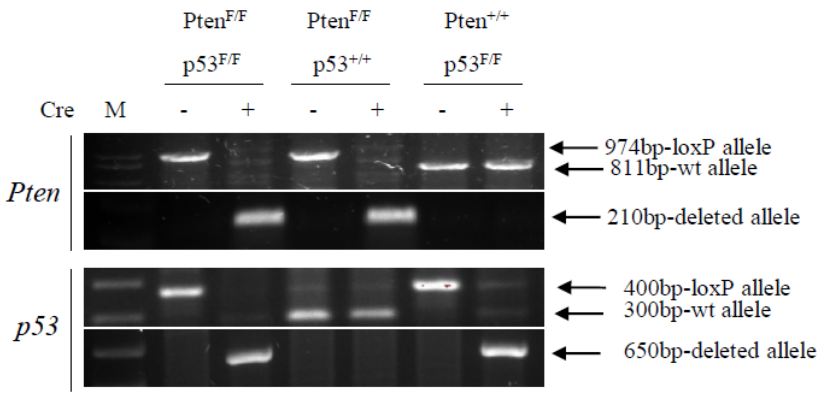

D

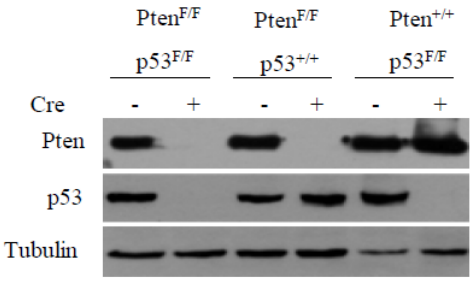

Figure S2 -Related to Figure 1

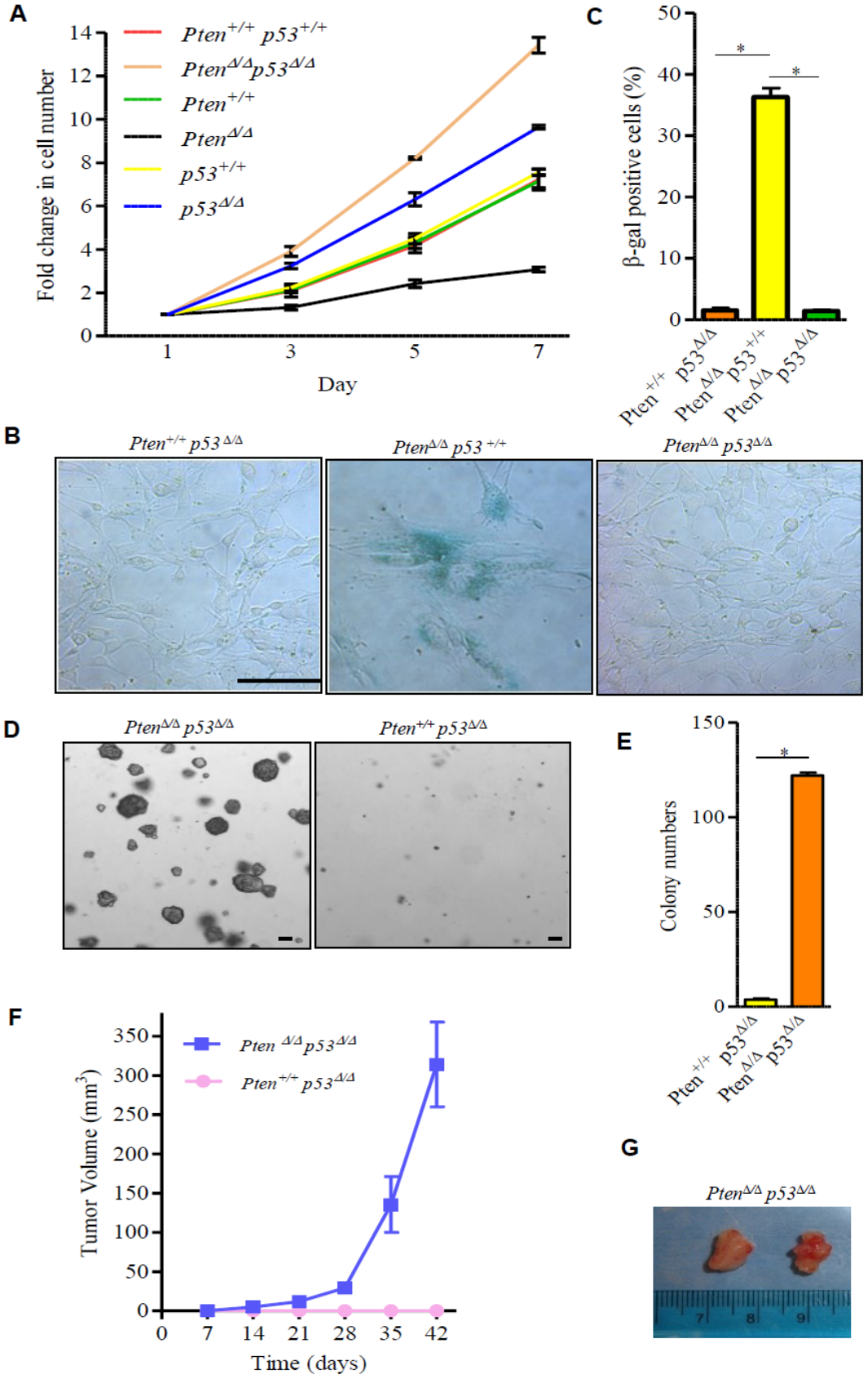

Figure S3 -Related to Figure 2

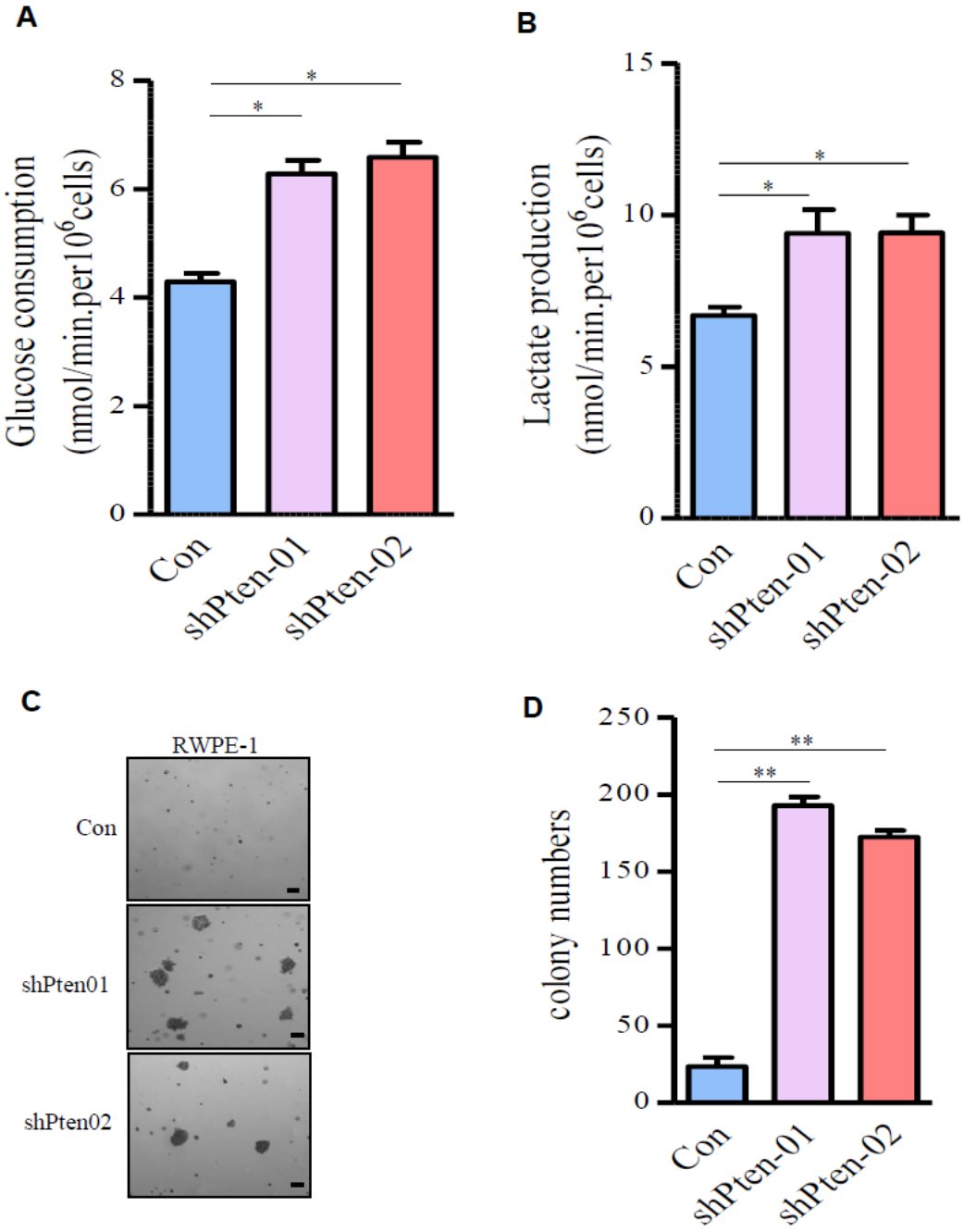

Figure S4 -Related to Figure 2

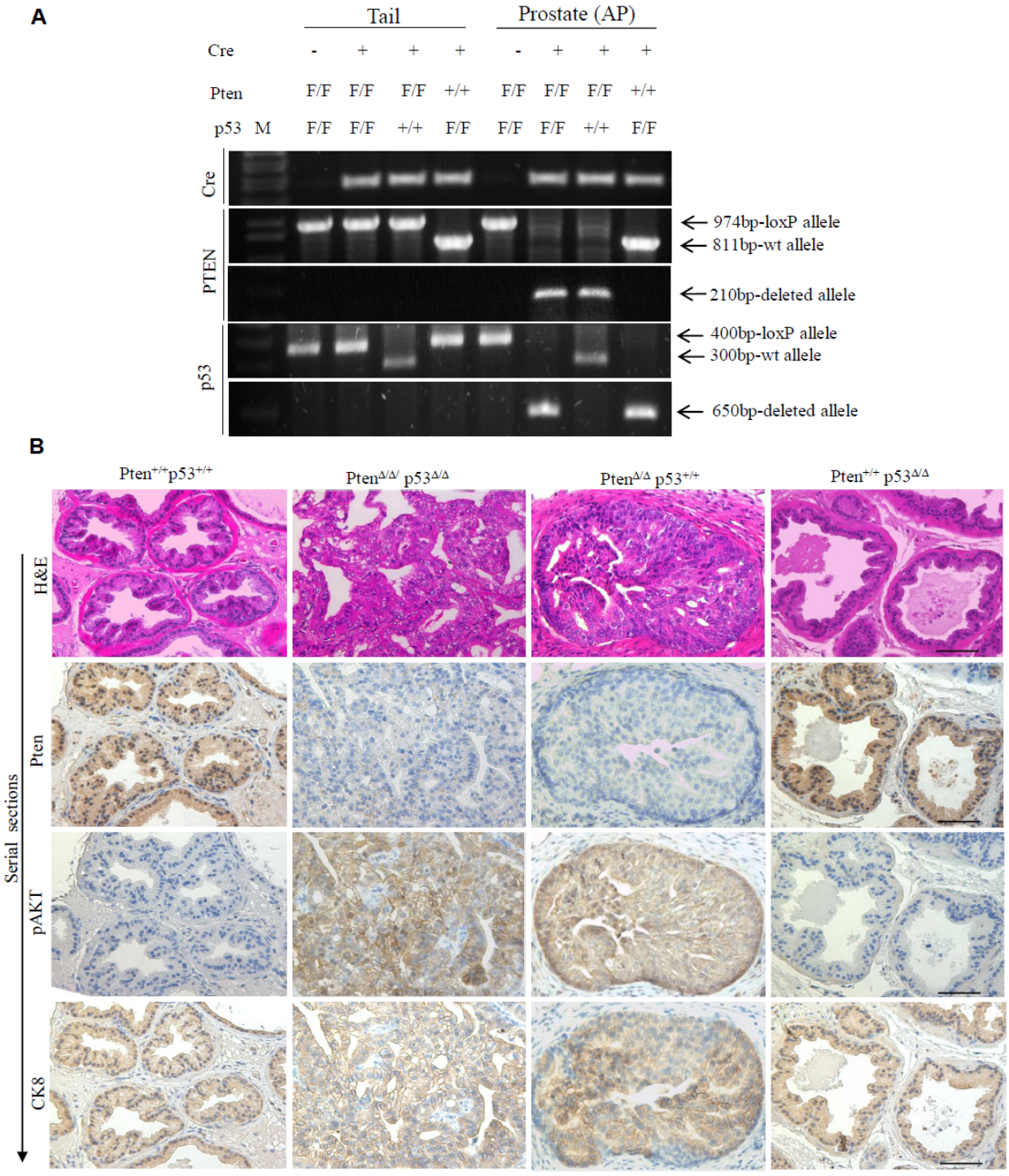

Figure S5 -Related to Figure 2

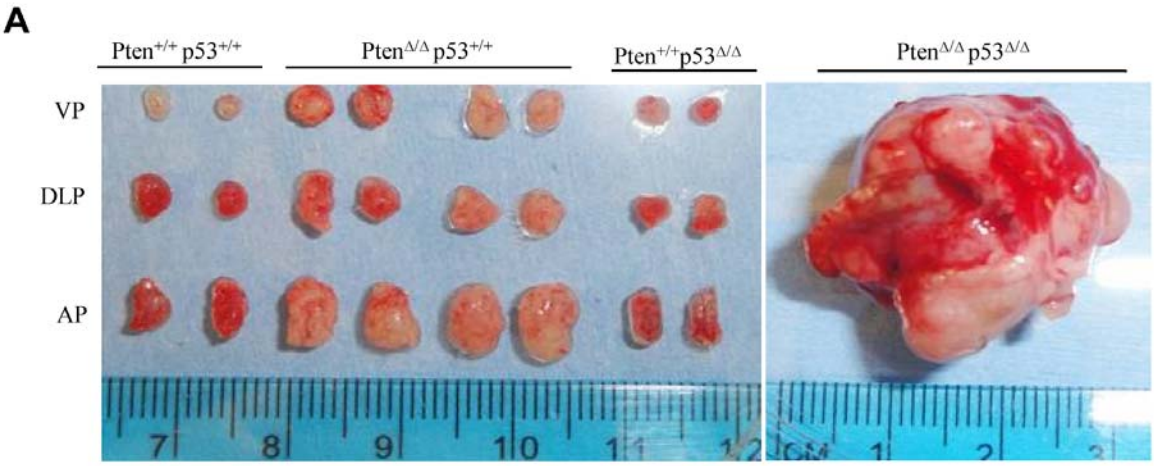

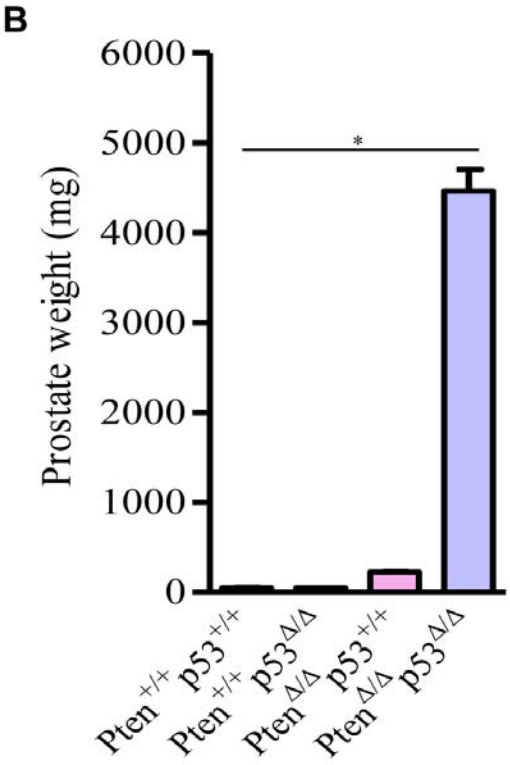

Figure S6-Related to Figures 3 and 4

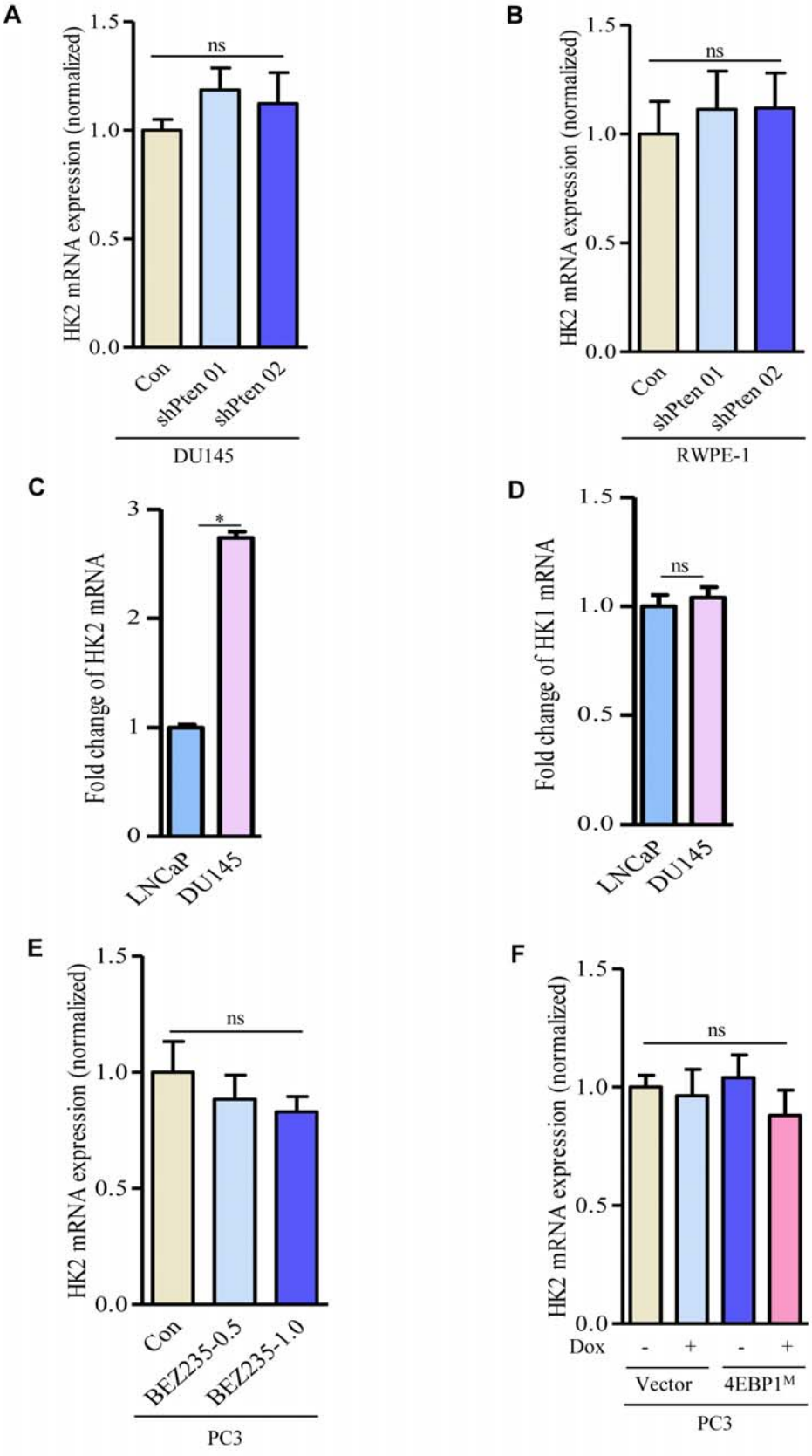

Figure S7-Related to Figure 7

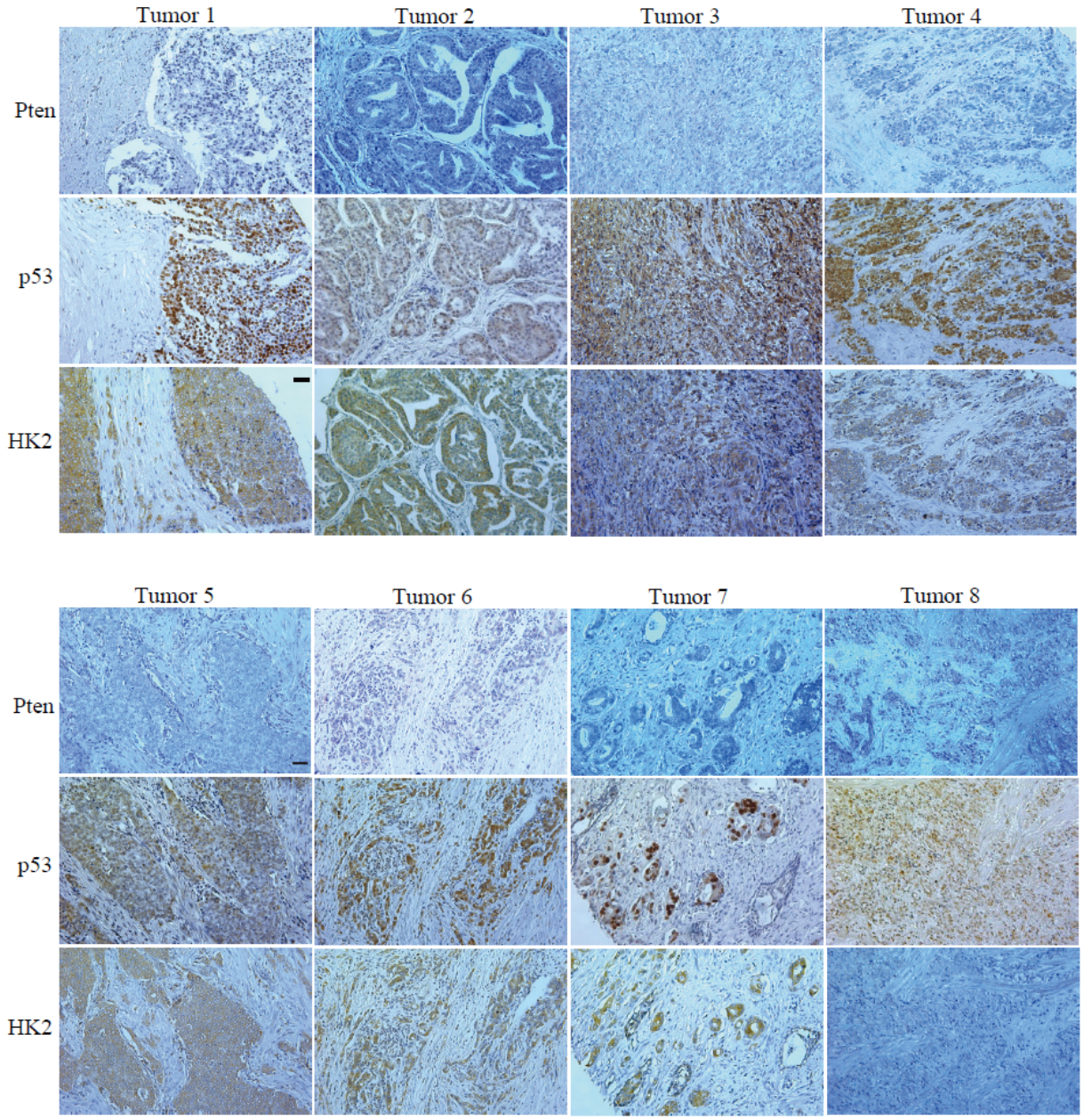

SUPPLEMENTAL FIGURE LENGENDS

Figure S1. Scheme of *Pten* and *p53* Conditional Knockout Alleles, Related to Figure 1. (A and B) Conditional knockout scheme for *Pten* (A) and *p53* (B) before and after Cre-mediated recombination with location of loxP (black triangles). (C) Genotyping PCR reactions. The *Pten* primers generated an 811 bp product for WT allele and a 974 bp product for the conditional knockout allele. The *p53* primers generated a 300 bp product for WT allele and a 400 bp product for the conditional knockout allele. In cells where Cre has been expressed, there would be a 210 bp and 650 bp product specific for the deleted *Pten* and *p53* allele, respectively. (D) Pten and p53 are detected by Western blot in MEFs with the indicated genotypes before and after Cre-mediated recombination. Tubulin serves as a loading control.

Figure S2. Loss of *Pten* and *p53* Promotes MEFs Transformation and Tumorigenesis, Related to Figure 1. (A) Growth curves of primary MEFs with the indicated genotypes. The error bars represent SEM (n=3). (B) MEFs with indicated genotypes were stained by SA-β-galactosidase for cellular senescence. (C) Quantification of SA-β-gal-positive cells from B. The error bars represent SEM. (D and E) Cells were plated in soft agar and colonies were counted after 21 days. Representative images of colonies are shown (D). Bar graph shows the average number of colonies (± SEM) from three independent experiments (E). (F and G) Xenograft tumor growth assay. 1 x 10^6 cells were injected subcutaneously to the lower flank of NSG mice. Tumor volumes were measured once per week and plotted as a function of time. Each data point represented average tumor volume (means ± SD) for the indicated genotypes (F), and representative images of tumors 6 weeks after injection are shown (G). P value was calculated using two-sided Student's *t* test. *P≤001. Scale bar, 100 um.

Figure S3. Depletion of *Pten* in RWPE-1 Cells Promotes Glycolysis and Cell Transformation, Related to Figure 2. (A and B) Glucose consumption (A) and lactate production (B) in control and *Pten*-depleted RWPE-1 cells. (C and D) RWPE-1 cells stably expressing control or shRNAs targeting *Pten* were plated in soft agar and colonies were counted after 21 days. Representative images of colonies growing in soft agar are shown (C) and quantification of colony formation in control and *Pten*-depleted RWPE-1 cells from three independent experiments (D). Data are shown as means ± SEM (n=3). P value was calculated using two-sided Student's *t* test. *P≤0.05. **P⩽001. Scale bar, 100 um.

Figure S4. Genetic Deletion of *Pten* and/or *p53* in Mouse Prostate, Related to Figure 2. (A) Genotyping PCR reactions of DNA from mouse tail and prostate. The *Pten* primers generated an 811 bp product for WT allele and a 974 bp product for the conditional knockout allele. The *p53* primers generated a 300 bp product for WT allele and a 400 bp product for the conditional knockout allele. The use of PB-Cre4 transgenic mice afforded prostate-specific expression of Cre recombinase. In prostate tissues where Cre had been expressed, there was a 210 bp and 650 bp product specific for the deleted *Pten* and *p53* allele, respectively. (B) Representative IHC images of H&E-, Pten-, pAKT- and CK8-stained prostate epithelial compartments of 20-week-old mice of the indicated genotype. Scale bar, 100 um.

Figure S5. Loss of *Pten* and *p53* in Prostate Epithelial Cells Causes Invasive Prostate Cancer *in vivo,* Related to Figure 2. (A) Representative images of prostate tumors from 20-week-old mice of the indicated genotypes. Except for $Pten^{\Delta/\Delta}p53^{\Delta/\Delta}$ mice, the prostate tumors could be separated into three prostatic lobes: anterior prostate (AP), ventral prostate (VP) and dorsolateral prostate (DLP). (B) Quantification of prostate weight (milligram) in the indicated

genotypes (n=6). Data are presented as mean ± SEM. P values were determined by a two-tailed Student's t test. *P≤0.01.

Figure S6. Effects of PTEN-AKT-mTORC1-4EBP1 Signaling on HK2 mRNA Expression, Related to Figures 3 and 4. (A and B) HK2 mRNA expression in DU145 cells (A) or RWPE-1 cells (B) with control or shRNAs targeting *Pten* were detected by real time RT-PCR. (C and D) Expressions of HK2 mRNA (C) and HK1 mRNA (D) in LNCaP and DU145 cells were determined by real time RT-PCR. Data are presented as mean ± SEM. (E) HK2 mRNA expression in control or BEZ235-treated PC3 cells. (F) HK2 mRNA expression in PC3 cells carrying tetracycline-inducible $4EBP1^{M}$. P values were determined by a two-tailed Student's t test. *P≤001. ns: not statistically significant.

Figure S7. HK2 Is Expressed in Human Prostate Cancers Carrying Pten and p53 mutations, Related to Figure 7. IHC representative images of HK2 protein expression in human prostate cancer samples with negative Pten ($Pten^{N}$) and positive mutant p53 ($mp53^{P}$) were shown. Note: No or very low expression of HK2 protein was detected in tumor 8. Scale bar: 100um.